Seismic response tests and analytical assessment of blind bolted assembly CFST frames with beam-connected SPSWs

Seismic response tests and analytical assessment of blind bolted assembly CFST frames with beam-connected SPSWs

Beibei Li [a], Jingfeng Wang [a,b*], Yong Lu [c], Zengde Zhang [a], Jiaxin Wang [a]

[a] *School of Civil Engineering, Hefei University of Technology, Anhui Province, 230009, China*
[b] *Anhui Civil Engineering Structures and Materials Laboratory, Anhui Province, 230009, China*
[c] *Institute for Infrastructure and Environment, School of Engineering, the University of Edinburgh, Edinburgh EH9 3JL, UK*

* Correspondence address: School of Civil Engineering, Hefei University of Technology, Anhui Province, 230009, China. Tel: 86 551 62901434, Fax: 86 551 62901434, E-mail address: jfwang008@163.com (J-F Wang)

Abstract: This paper presents a series of experimental and analytical studies to investigate the seismic behavior of blind bolted assembly concrete filled steel tube (CFST) frames with infill steel plate shear walls (SPSWs) connected to beam only. Two specimens of single-bay, two-story blind bolted assembly CFST frames with beam-connected SPSWs were fabricated and tested under lateral cyclic load combined with a constant vertical axial load. The test parameters include the column section type, the beam-SPSW connection type and the SPSW setting. Typical failure modes of the specimens were summarized and discussed. The test results show that the presence of SPSWs can compensate effectively the relatively small lateral stiffness of bare blind bolted CFST frames, and the novel SPSW-frame system exhibited good hysteretic performance, ductility and energy dissipation capacity. Moreover, the moments at the beam ends of a CFST frame with semi-rigid joints under two partial vertical loads resulting from the beam-connected SPSWs are derived. A practical design method for semi-rigid CFST frames with beam-connected SPSWs is summarized for checking the strength of blind bolted end plate joints, steel beams and CFST columns. The accuracy of the design method is also verified by the test results. The study shows that the novel SPSW-frame has good potential for application in earthquake resistant design of steel frame structures.

Keywords: Steel plate shear walls (SPSWs); Concrete-filled steel tube (CFST); Steel frames; Blind

bolted end plate joint, Seismic behavior

1 Introduction

Steel plate shear walls (SPSWs) have seen increased application in medium- and high-rise buildings in seismic active regions. The framed steel plate wall has advantages of high stiffness, good ductility, stable energy dissipation capacity, low seismic mass and fast construction. In a typical frame infilled with steel plate walls, the SPSWs are welded or bolted to the boundary beams and columns of the frame, and as a result the overall mechanical performance of the system is similar to a vertical cantilever plate beam. Prior to 1980s, the infill plate was designed as either a thick or a stiffened steel plate to avoid the local buckling of the plate [1]. However, such an approach was costly and the constructability was low in comparison with traditional reinforced concrete (RC) shear walls. In recent years, the concept of making full use of the post-buckling strength of SPSWs has been proposed and studied by many researchers [2-13]. The research results have shown that the unstiffened thin steel plates tend to buckle during the early stages of lateral loading and then develop a diagonal tension field action to resist lateral load efficiently. Therefore, the SPSWs can be applied as good earthquake-resistant systems with high load carrying capacity and ductility.

However, SPSWs with all edges connected to the boundary frame members may lead to columns suffering from large bending moments, and this could lead to early failure of columns and consequently incomplete utilization of the full seismic performance capacity of SPSWs. Therefore, connecting the SPSWs to frame beams only has been proposed by some scholars [14-25] as a possible solution to the above issue. This typological form of SPSWs eliminates the dependence on columns, and at the same time reduces the field installation workload. In addition, the door or window openings can be conveniently arranged for this kind of SPSWs.

Xue and Lu [14, 15] firstly proposed the SPSWs with two-side connections and conducted analytical studies. Choi and Park [16] carried out five three-story, single-bay H-shaped steel frames

with thin plates to investigate the effects of various infill plates on the structural capacity. Vatansever and Yardimci [17] completed experiments on two SPSWs infilled H-shaped steel frames with semi-rigid joints. Guo et al. [18, 19] presented successively the study of beam-connected SPSWs and corresponding SPSWs infilled rigid concrete-filled steel tube (CFST) frames. Clayton et al. [20, 21] reported a series of cyclic tests to understand the self-centering SPSWs and component behavior, and subsequently Ozcelik and Clayton [22, 23] further studied the strip model and seismic performance of beam-connected SPSWs designed for low-seismic regions. The seismic behavior of beam-connected SPSWs were also studied by Shekastehband et al. [24, 25]. The above mentioned studies showed that the beam-connected SPSWs exhibited significant lateral resistance, energy dissipation and ductility.

On the other hand, in order to ensure force transfer between the SPSWs and the boundary members, welded connections are generally used along four or two edges of the SPSWs. However, the thickness of SPSWs is usually between 1 and 6 mm, making the welding difficult to execute on-site with good quality control, and the labor cost for the use of the full welded connections is also very high. Moreover, experimental investigations [5-8, 16, 19, 20] on the SPSWs which were welded to boundary members found that initial tearing mostly occurred at the welds around the corners of the infill SPSWs. This initial tearing usually propagated along the boundary members, leading to degraded energy dissipation of SPSWs as compared to bolted connections. Using bolted connections has a further advantage in that removing damaged SPSWs is easier. In view of all the above and for fast fabrication and reliable SPSW-boundary member connections, bolted connections may be required in the SPSW systems.

For the main frame itself, it is generally recognised that the CFST columns may be used as a good alternative to conventional H-shaped members in terms of withstanding combined high axial load and flexural moment. Thus, there are merits of using CFST columns in SPSW-infilled frames to satisfy the stiffness and strength requirements.

In a separate development, a novel blind bolted assembly CFST frame has been proposed [26-29]

amid the drive towards building industrialization and for its excellent seismic performance. In a blind bolted assembly CFST frame, the steel beams are fixed to the circular or square CFST columns by blind bolts and end plates, and the bolts can be fastened from the outside of the hollow section column, as shown in Fig. 1. Compared with fully welded or web-bolted flange-welded joints, the blind bolted end plate joints avoid the inconvenience of extensive welding while still maintain excellent dissipation and remarkable ductility [26-42]. Previous studies [26-42] demonstrated that the blind bolted end plate joints showed a semi-rigid feature and provided a reasonable degree of continuity and optimization of the moment distribution in frame structures. However, it should be noted that the lateral stiffness of the blind bolted assembly CFST frames is generally smaller than those of rigid CFST frames, and this poses limitation of their application in high- and super high-rise buildings.

At this juncture, it appears to be clear that bringing the SPSWs to blind bolted assembly CFST frames could be a good solution. However, so far there has been little research on this potentially promising topic. Vatansever and Yardimci [17] studied a related topic on the cyclic performance of semi-rigid H-shaped steel frames with beam-connected SPSWs, and Dubina and Dinu [43] and Guo [44, 45] studied the seismic behavior of semi-rigid H-shaped steel frames with fully connected SPSWs. There is currently no direct study on the structural performance of the blind bolted assembly CFST frames with beam-connected SPSW under seismic loading.

This study is therefore focused on a novel combination of the blind bolted assembly CFST frames with SPSW infills connected to beams only. The main purpose of the present paper is to investigate the seismic behavior of such a combined frame system under cyclic loading by experimental and theoretical studies. Two single-bay, two-story specimens of the CFST-SPSW systems have been conducted to examine the failure mechanisms and hysteretic behavior. The stiffness degradation, ductility and energy dissipation of the novel CFST-SPSW system are analyzed in detail. The effects of the column section type, beam-SPSW connection type and SPSW setting on the seismic-resistant behavior of the frame system are also investigated. On this basis, a practical

design method for blind bolted assembly CFST frames under partial tension field action resulting from beam-connected SPSWs has been summarized for checking the strength of the blind bolted end plate joints, steel beams and CFST columns. The accuracy of the design method is verified experimentally.

2 Experimental program

2.1 Test specimens

In order to evaluate the associated seismic behavior of the new SPSW system, two one-third scale models of two-story, single-bay blind bolted end plate CFST frames with beam-connected SPSWs were designed and tested. Table 1 lists the dimensions of the boundary members, thickness of the infill plates, SPSW-beam connection type and beam-column joint type. The detailed configurations of the specimens are shown in Fig. 2. The height of first and second story was 1475 mm and 1550 mm, respectively, and the span was 2000 mm between column centerlines for both specimens. The columns for specimen CFW1 were concrete-filled circular steel tubes with a cross-section of 200 mm in diameter and 8 mm in thickness, and the columns for specimen SFW1 were concrete-filled square steel tubes with a cross-section of 200 × 200 × 8 mm. The H-shaped steel beams of all specimens were designed with larger flexural rigidity (300 × 150 × 6.5 × 9 mm), so that they can provide relatively strong constraint boundary conditions to ensure the SPSWs can make a large amount of contribution to the overall strength and stiffness of this type of system. The steel beams and columns were connected using end plates and blind bolts. Two types of end plate beam-column joints were employed in the experiment, namely extended end plates in the first story and flush end plates in the second story.

Self-consolidating concrete mix was filled in the circular or square steel tubular columns after the erection of steel framework. The steel beams with end plates were fastened to circular or square steel tubular columns by blind bolts with hooked extensions into the concrete core, as shown in Fig. 1. The hooked extensions were welded to the head of the bolt to resist the bolt heads pulling

through.

In order to investigate the influence of different SPSW-beam connection types, in the first story of both specimens, the infill SPSWs were 1275 mm high, 1760 mm long and 5 mm thick, and they were connected on the upper and lower horizontal edges to beams by 125 × 80 × 8 mm steel angles and M20 high-strength bolts (Fig. 2 (e) and (f)). On the other hand, in the second story for both specimens, the SPSWs were 1210 mm high, 1760 mm long and 5mm thick, and they were welded to the boundary beams using 8-mm-thick and 120-mm-wide fish plates (Fig. 2 (f) and (g)).

2.2 Cyclic loading apparatus

The test setup is depicted in Fig. 3. Both specimens were tested under cyclically increasing lateral load while a constant axial load was applied on the CFST columns. Two 2000-kN hydraulic jacks were installed at the upper end of the columns to apply the vertical (axial) loads. An MTS servo-electrical controlled hydraulic actuator with 1000 kN capacity was used to apply in-plane reversed loads to simulate seismic loading. The axial load ratio of the CFST columns was selected as 0.3. The 'Positive Direction' and 'Negative Direction' of displacement and load were illustrated in Fig. 3(a).

The cyclic loading protocol was determined based on ATC-24 guidelines [46], as shown in Fig. 4. For the elastic phase three horizontal displacement levels were chosen at $0.25\Delta_y$, $0.5\Delta_y$ and $0.7\Delta_y$, respectively, and each level contained two cycles. The yielding displacement, Δ_y, was calculated theoretically and rounded to 20 mm. The intermediate phase consisted of four displacement levels at $1.0\Delta_y$, $1.5\Delta_y$, $1.75\Delta_y$ and $2.0\Delta_y$, respectively, and each level contained three cycles. The advanced inelastic phase had increments at $2.25\Delta_y$, $2.5\Delta_y$, $3.0\Delta_y$ and $3.5\Delta_y$, respectively, and at each level two cycles were performed.

Strain gauges were mounted on the critical points of the steel beams, steel tubes, end plates and SPSWs to obtain the strain distribution. A total of 74 strain gauges were employed on each of the

specimens. The layout of the strain gauges is illustrated in Fig. 5.

2.3 Material properties

Steel coupons were tested to determine the yield stress (f_y), ultimate stress (f_u), Young's modulus (E), and elongation at fracture (δ). The results are summarized in Table 2. The yield and ultimate strength of the Grade 10.9 M20 bolts were found to be 923 N/mm^2 and 1012 N/mm^2, respectively.

The cube compressive strength of concrete was determined from testing standard concrete cubes of 150 × 150 × 150 mm, and the modulus of elasticity was determined from concrete cubes of 150 × 150 × 300 mm. Three groups of concrete cubes were tested and each group had three specimens. The average ultimate compressive cube strength was found to be 53.62 MPa and the modulus of elasticity was 34.6 GPa.

3 Experimental results and analysis

3.1 Failure modes

In both specimens, a small diagonal buckling wave was observed in the SPSWs at the first and second stories during the loading cycles of $0.5\Delta_y$ and $0.7\Delta_y$, due to a compressive state and the fact that there was no restraint effect from columns to the infill plates. When the horizontal displacement reached 20 mm or $1.0\Delta_y$, residual deformation appeared firstly in the upper SPSWs and the affected plates could not return to a flat state when the lateral displacement returned to zero. A similar phenomenon occurred to the lower SPSWs during the loading cycles of $1.75\Delta_y$ and $2.0\Delta_y$.

The expansion of the diagonal tension field and buckling waves become more and more obvious with incremental reversed cycles. For specimen CFW1, when the top displacement increased to 70 mm or $3.5\Delta_y$, two main diagonal buckling waves emerged in the upper SPSW and the wave height was 40 mm, and meanwhile the middle left part of the upper SPSW concaved to north about 90 mm (Fig. 6 (a) and (b)). For specimen SFW1, when the top displacement reached 60 mm or $3\Delta_y$, the maximum out-of-plane deformation measured at about 80 mm and 60 mm in the upper and lower

SPSWs, respectively (Fig. 7 (a) and (b)). In addition, the rumbling sound could be heard intermittently during the whole loading process, especially when the loading direction changed from negative to positive. This was mainly attributed to the deformation of the SPSWs and the slip of the bolted connections.

In the test process, the end plates and walls of CFST columns were still in contact with each other around the location of blind bolts, although the end plates buckled between the gap of two rows of blind bolts. At the same time, the blind bolts had not been pulled out from the column wall. The phenomena, to some extent, showed the reliability of this type of joint using blind bolts. The maximum deformation of the extended end plates in specimen CFW1 and SFW1 was respectively about 9 mm and 6 mm, as seen in Fig. 6 (c) and Fig. 7 (c). It showed that the blind bolts had a robust performance under a strong earthquake action.

Meanwhile, bending deformation can be observed in the bottom flanges of the top steel beams after the tests, as depicted in Fig. 6 (b) and Fig. 7 (b). In addition, the fish plates located at the intermediate beams inclined to north on account of the out-of-plane force of infill plates acting on the fish plates. When the horizontal displacement increased to 70 mm and 60 mm for specimen CFW1 and SFW1, respectively, welding seam fracture occurred at the bases of CFST columns of both specimens, as illustrated in Fig. 6 (d) and Fig. 7 (d). At the same time, the overall out-of-plane deformation of the test frame occurred. Therefore, the test was terminated for safety reasons. In the practice, engineers can design several stiffeners at the CFST column base, at the same time, concrete can also be poured around the CFST column base to further strengthen the column base. On the other hand, if this type of structure system can be designed reasonably, the end plates and SPSWs would undergo larger deformation and even damage after a moderate earthquake, so they may need to be replaced to meet the needs of buildings under the serviceability limit state.

3.2 Load versus top drift hysteretic curves

To facilitate a comparison between the seismic behavior of blind bolted assembly CFST frames infilled with beam-connected SPSWs and bare blind bolted CFST frames, the recorded cyclic

curves of lateral load versus top drift for all specimens with and without SPSWs are shown in Fig. 8. The hysteretic curves of specimens without SPSWs were described in Wang et al. [29]. The dimensions of specimens SCF1 and SSF1 are same as specimens CFW1 and SFW1, respectively, in terms of CFST columns, steel beams and blind bolted end plate joints. Meanwhile, the steel and concrete of four specimens were from the same batch.

As illustrated in Fig. 8 (a) and (b), the lateral load resistance of both specimens increased with an increase of the lateral drift, while the slope of curves began to decrease and the strength degradation can also be observed at the same loading level. This was mainly attributed to the tension strips and buckling performance. The lateral load-drift curves of specimen CFW1 and SFW1 had little pinching effect as compared to bare specimens, but the blind bolted CFST frames with beam-connected SPSWs still possessed consistent loading resistance and stable energy dissipation.

As can be observed from Fig. 8 (a) and (b), although the bare specimens showed a more stable response and lager lateral drift, specimens CFW1 and SFW1 exhibited higher initial stiffness and larger lateral load resistance as compared with those of specimen SCF1 and SSF1 reported in [29]. These results demonstrated that the infill SPSWs can effectively increase the initial stiffness and lateral load resistance.

4 Evaluation of cyclic behavior

4.1 Load versus top drift skeleton curves

The lateral load vs. top drift skeleton curves of the test specimens are constructed by tracing the maximum load point at each loading level according to the hysteretic curves. The results are shown in Fig. 9. The effect of the column section type and the SPSW setting on the strength capacity and elastic stiffness of the frames can be clearly observed. Table 3 lists the yield load, the maximum load, the failure load and the corresponding displacements. The yield load (P_y) and yield

displacement (Δ_y) are determined as depicted in Fig. 10. A tangent is drawn at the coordinate system origin and the intersection between the tangent and the horizontal line of the maximum load is defined as the yield displacement (Δ_y). The intersection between the vertical line and the skeleton curve is defined as the yield load (P_y). The maximum point is identified by the maximum lateral load and corresponding displacement in the positive or negative direction. The failure point is determined when load reduces to 85% of the maximum load or when the test was terminated.

According to the characteristic points of the skeleton curves, the maximum lateral resistant load of specimen SFW1 was slightly (about 2%) lower than that of specimen CFW1. Comparing to the bare frame counterpart, the circular blind bolted CFST frames CFW1 achieved a maximum lateral resistance which was 94~97% larger than SCF1, while the square blind bolted CFST frame SFW1 achieved a maximum lateral resistance which was 41~62% larger than SSF1. These results showed that the presence of the infill SPSWs worked effectively in enhancing the lateral resistance. Meanwhile, the comparison between specimens CFW1and SFW1 indicated that the contribution of column section type to the lateral resistance was negligible, due apparently to the fact that the SPSWs possessed high elastic stiffness making the difference introduced by the column types less significant overall, although the inertia moment of square CFST column is larger than that of circular CFST column at the same width and steel ratio of column section.

4.2 Stiffness degradation

Another perspective of the cyclic behavior of the test specimens is provided using stiffness degradation factor (K_j). The stiffness degradation factor (K_j) of a composite structure is expressed as follows [47]:

$$K_j = \sum_{i=1}^{n} P_j^i \Big/ \sum_{i=1}^{n} u_j^i \tag{1}$$

where P_j^i is the peak lateral loads at the jth loading cycle; u_j^i is the corresponding lateral displacements; n is the number of cycles at each displacement level.

Fig. 11 shows the results of the stiffness degradation factor as a function of the top drift for the two test specimens. 'PD' and 'ND' mean 'Positive Direction' and 'Negative Direction', respectively, in Fig. 11. Progressive but considerable degradation can be observed in each specimen as the drift increases, due to the cumulative damage. The stiffness of specimen CFW1 at the elastic and failure stages were 21×10^3 kN/m and 10×10^3 kN/m, respectively, and corresponding values of specimen SFW1 were 22×10^3 kN/m and 12×10^3 kN/m, respectively. The comparative results between the two specimens showed that the column section type had little influence on the stiffness of the structure. It should be noted that due to the limitation of laboratory conditions, there was only one servo-electrical controlled hydraulic actuator exerting reversed loads on the second story. It was consequently difficult to get the exact load acting on the first story. This paper focused on the overall stiffness of the two-story specimens, although the specimens had different story stiffness values owing to the various connections used in the first and second stories.

However, comparing to the bare frames, the elastic stiffness of specimen CFW1 and SFW1 was respectively about 2.7 and 3.3 times, and the failure stiffness of specimen CFW1 and SFW1 was respectively about 3.8 and 3.3 times as much as that of specimen SCF1 and SSF1. This comparison demonstrates that the infill SPSWs contributed significantly to the initial stiffness and the post-shearing buckling of infill SPSWs still had stable stiffness. In addition, the rapid stiffness degradation could be observed in the SPSW specimens relative to the bare frame specimens. This was primarily because that the beam-connected SPSW can be easily buckled and deformed largely when specimens underwent increasing lateral displacement. Thus its stiffness decreases rapidly.

4.3 Ductility and energy dissipation

Ductility refers to the ability of a structure or a member to undergo inelastic deformation without significant reduction in its load carrying capacity. Ductility is of similar importance as strength in the structural earthquake-resistant design. In this section the displacement ductility ratio (μ) is examined for the new SPSW-frame system.

The displacement ductility ratio (μ) is defined as the ratio of the ultimate (failure) state displacement (Δ_f) to the yield state displacement (Δ_y):

$$\mu = \Delta_f / \Delta_y \tag{2}$$

The displacement ductility ratios (μ) of both test specimens are also listed in Table 3. The ductility is in a range of 2.27 to 2.43. The results also show that the effect of the column section type on ductility ratio was negligible. It should be noted that the specimens could actually continue to undertake further increased displacement, however due to premature welding seam fracture at the base of the CFST columns and the overall instability, the loading process had to be terminated. So the ductility ratios given above may be regarded as representing a lower bound that the new frame system can achieve. In terms of the story drift, its lowest value was 1.94% and this is very close to 2%, which is a general elastic-plastic story drift limit for steel building structures in the design for strong earthquakes.

Fig. 12 presented the energy absorbed at each loading level, which is calculated by the area enclosed by the hysteresis loop. As expected, the energy dissipation of the blind bolted CFST frames with SPSWs was 2-2.5 times larger than that of the bare blind bolted CFST frames at the same drift demands. The column section type exhibited some influence on the energy dissipation of the bare frames, whereas it showed little effect on the energy dissipation for the frames infilled with SPSWs. It can be seen that while the energy dissipated is larger at each loading protocol, the ductility of the system is reduced.

5 Mechanics of beam-connected SPSW with semi-rigid joints

In order to accurately simulate and calculate the behavior of fully-connected SPSWs, the strip model was originally proposed by Thorburn et al. [48] where a series of inclined tension-only truss elements with a uniform loading are used to represent the diagonal tension field of the steel plate. Meanwhile, the strip model could also be used in beam-connected SPSWs. Fig. 13 shows an analytical model for the interaction between a pair of SPSWs and the beam to which the SPSWs are connected. The beam is jointed at both ends to CFST columns through blind bolts and end plates. Under lateral deformation, partial tension fields (PTFs) develop on the top and bottom sides of the beam over the diagonal portions of the SPSWs being restrained by the respective sides of the beam. Experimental and analytical studies on beam-connected SPSWs [14-25] have verified the existence of PTFs and indicated that the results between experiments and predictions could match well with each other using the strip model.

For a typical CFST frame beam with blind bolted end plate joints, the beam end moment (M_{bi}) should always be smaller than the moment resistance of the joints (M_{ju}) to avoid premature failure of the joints during seismic loading. Under two partial uniformly distributed loads resulting from the beam-connected SPSWs, the beam end moment (M_{bi}) can be derived through the beam end rotation (θ_{bi}), which in turn can be determined as the sum of four portions, as seen in Fig. 14:

(1) rotation of the corresponding simple beam under a partial uniformly distributed load applied on the top side, $\theta_{qy(i+1)}$;

(2) rotation of the corresponding simple beam under a partial uniformly distributed load applied on the bottom side, θ_{qyi};

(3) rotation of the simple beam under the moment at the left end of the beam, $\theta_{Mi,l}$; and

(4) rotation of the simple beam under the moment at the right end of the beam, $\theta_{Mi,r}$. Hence,

$$M_{bi,l} / R_{ki,l} = \theta_{bi,l} = \theta_{qy(i+1),l} + \theta_{qyi,l} + \theta_{M_{bi,l},l} + \theta_{M_{bi,r},l} \tag{3}$$

$$M_{bi,r} / R_{ki,r} = \theta_{bi,r} = \theta_{qy(i+1),r} + \theta_{qyi,r} + \theta_{M_{bi,l},r} + \theta_{M_{bi,r},r} \tag{4}$$

where $M_{bi,l}$ and $M_{bi,r}$ are the moments at the left and right end of the beam, respectively; $R_{ki,l}$ and $R_{ki,r}$ are the corresponding connection stiffness of the blind bolted end plate joints. Subscript i denotes the floor number for the beam under consideration.

Substituting each rotation into Eq. (3) or (4) and integrating, the moment at the left and right end of the beam with blind bolted joints can be expressed ad as

$$M_{bi,l} = (-\lambda_{i,l}\frac{q_{y(i+1)}L_{i+1}^2}{2}\phi_{2i} - \frac{q_{y(i+1)}L_{i+1}^2 L_{bi}}{4}\phi_{1i} + \lambda_{i,l}\frac{q_{yi}L_i^2}{2}\psi_{1i} + \frac{q_{yi}L_i^2 L_{bi}}{4}\psi_{2i}) / (4\lambda_{i,l}^2 L_{bi}^2 - L_{bi}^4) \quad (5)$$

$$M_{bi,r} = (\lambda_{i,r}\frac{q_{y(i+1)}L_{i+1}^2}{2}\phi_{1i} + \frac{q_{y(i+1)}L_{i+1}^2 L_{bi}}{4}\phi_{2i} - \lambda_{i,r}\frac{q_{yi}L_i^2}{2}\psi_{2i} - \frac{q_{yi}L_i^2 L_{bi}}{4}\psi_{1i}) / (4\lambda_{i,r}^2 L_{bi}^2 - L_{bi}^4) \quad (6)$$

where $\phi_{1i} = 2L_{bi}^2 - L_{i+1}^2$; $\phi_{2i} = (2L_{bi} - L_{i+1})^2$; $\psi_{1i} = 2L_{bi}^2 - L_i^2$; $\psi_{2i} = (2L_{bi} - L_i)^2$; $\lambda_{i,l} = (1 - r_{i,l} - r_{i,l}L_{bi}) / r_{i,l}$; $\lambda_{i,r} = (1 - r_{i,r} - r_{i,r}L_{bi}) / r_{i,r}$. Note that the moment is defined as positive when it rotates clockwise around the end of the beam.

Xu and Grierson [49] and Simões [50] proposed the concept of end-fixed factor (r_i) to express the relationship between the connection stiffness and the beam linear stiffness, which was defined as:

$$r_{i,l} = \frac{1}{1 + (3EI_{bi} / R_{ki,l}L_{bi})}, \quad r_{i,r} = \frac{1}{1 + (3EI_{bi} / R_{ki,r}L_{bi})} \quad \text{.....(7)}$$

where I_{bi} is the moment of inertia of the beam; L_{bi} is the net length of the beam and also equals to the length of SPSWs in this paper; $R_{ki,l} = S_{ki,l} / 2$ and $R_{ki,r} = S_{ki,r} / 2$ are given in accordance with EC3 Appendix J [51]; S_{ki} is the initial stiffness of blind bolted end plate joints to CFST columns.

It can be seen that when the beam-column joint is pinned, $r_i = 0$; when it is rigid, $r_i = 1$; and when it is semi-rigid, $0 < r_i < 1$.

For beam-connected SPSWs in a multi-story frame that satisfactorily develop the uniform yielding over the PTF length, the distributed horizontal and vertical loads applied along the i-th and (i+1)-th story beams (q_i and q_{i+1}) are important internal forces to be considered in the design of the boundary members. These distributed loads can be calculated using the following equations [1, 22]:

$$q_{yi} = 0.5 f_{y,wi} t_{wi} \sin(2\theta_i) \quad q_{y(i+1)} = 0.5 f_{y,w(i+1)} t_{w(i+1)} \sin(2\theta_{i+1})$$
$$q_{xi} = f_{y,wi} t_{wi} \cos^2(\theta_i) \quad , \quad q_{x(i+1)} = f_{y,w(i+1)} t_{w(i+1)} \cos^2(\theta_{i+1}) \tag{8}$$

$$L_i = L_{bi} - H_{wi} \tan\theta_i \quad , \quad L_{i+1} = L_{bi} - H_{w(i+1)} \tan\theta_{i+1} \tag{9}$$

$$\theta_i = \gamma_i \tan^{-1}(L_{bi} / H_{wi}) \quad , \quad \theta_{i+1} = \gamma_{i+1} \tan^{-1}(L_{b(i+1)} / H_{w(i+1)}) \tag{10}$$

$$\gamma_i = 0.55 - 0.03(L_{bi} / H_{wi}) \geq 0.51 \quad , \quad \gamma_{i+1} = 0.55 - 0.03(L_{b(i+1)} / H_{w(i+1)}) \geq 0.51 \tag{11}$$

where $f_{y,wi}$ and $f_{y,w(i+1)}$ are the yield strength of the SPSWs at the i-th and (i+1)-th stories, respectively; t_{wi} and $t_{w(i+1)}$ are the thickness of the SPSWs at the i-th and (i+1)-th stories, respectively; other parameters have been illustrated in Fig. 13.

In order to calculate the beam end moment (M_{bi}), the initial stiffness (S_{ki}) of the blind bolted end plate joint should be worked out. It can be calculated through the component method. In this method, the joint is partitioned into a set of individual basic components. Each of the basic component represents part of the joint and can be replaced by a series of parallel simple spring elements, as shown in Fig. 15. The initial stiffness (S_{ki}) is given by the following equation [34, 52, 53]:

$$S_{ki} = \xi_s E k_{eq} z_{eq}^2 \tag{12}$$

$$\xi_s = \begin{cases} 1.0 & \text{for retangular section column} \\ 1.1 & \text{for circular section column} \end{cases} \tag{13}$$

where E is the Young modulus of the steel; k_{eq} and z_{eq} are the equivalent stiffness factor and equivalent lever arm, respectively.

$$k_{eq} = \sum_{j=1} k_{eff,j} z_j / z_{eq} \tag{14}$$

$$z_{eq} = \sum_{j=1} k_{eff,j} z_j^2 / \sum_{j=1} k_{eff,j} z_j \tag{15}$$

$$k_{eff,j} = 1/(1/2k_{csw} + 1/k_{cf} + 1/k_{ep} + 1/k_{bo}) \tag{16}$$

$$
\begin{aligned}
k_{csw} &= t_c\left[2.9\overline{t_c}^{-0.4}+1.1\overline{d_0}\right] \\
k_{cf} &= t_c\overline{t_c}^{-2}\frac{5\overline{d_0}+(9-10\overline{X_B}-278\overline{t_c}^{2})\tan\overline{X_B}}{\overline{X_B}^{3}-1.5\overline{X_B}^{2}+(0.464+\overline{t_c})\overline{X_B}+0.092-\overline{t_c}} \\
k_{ep} &= 0.9l_{eff}\left(t_{ep}/m_{ep}\right)^3 \\
k_{bo} &= 1.6A_{bo}/l_{bo}
\end{aligned}
\tag{17}
$$

where $\overline{d_0}=d_0/h_c$; $\overline{X_B}=X_B/h_c$; $\overline{t_c}=t_c/h_c$; z_i is the distance from the bolt row j to the centre of beam bottom flange; $k_{eff,j}$ is the stiffness factor at bolt row j; k_{csw}, k_{cf}, k_{ep}, and k_{bo} are respectively the stiffness factors of the column side wall in tension, column face in bending, end plate in bending and bolt in tension; h_c and t_c are respectively the outer dimension and wall thickness of column section; d_0 is the diameter of bolt hole; l_{eff} is the smallest effective length according to EC3 [52]; t_{ep} is the end plate thickness; m_{ep} is the distance between the centre of the bolt hole and the beam web welding; A_{bo} and l_{bo} are respectively the effective cross-sectional area of bolt and the bolt elongation length. X_B is the horizontal spacing between bolts. Especially for the circular section column, X_B is the arc length between bolts along the wall surface of the column;

Previous experimental studies [34-42] on the blind bolted end plate joints to CFST columns showed that the initial stiffness and moment resistance of a joint with curved end plates were larger than those of a joint with flat end plates under the same bolt arrangement and dimension of end plate. This was mainly because of the restraining effect from curved end plates. As the joint was subjected to a moment, the tangential component forces along the arc surface of columns from the bolt pretension forces can restrain the deformation of curved end plates. This restraining effect would contribute in increasing the initial stiffness and the moment resistance for curved end plates in comparison with flat end plates. However, existing experimental and analytical studies have not paid attention to this phenomenon, and the corresponding formulas have not fully considered the restraining effect of the curved end plates.

To rectify this shortcoming, a stiffness restraint coefficient (ξ_s) and moment restraint coefficient

(ξ_m) are proposed in this paper to take into consideration the enhancement effect of the blind bolted joints to CFST columns with curved end plates on the joint stiffness and moment resistance.

Table 4 summarizes previous experiments on this type of joints and the corresponding results [34-42]. The stiffness and moment restraint coefficients in Table 4 are the ratios of the initial stiffness and moment resistance of the joints with curved end plates to the corresponding joints with flat end plates. The maximum and minimum values are excluded when calculating the mean and standard deviation of the coefficients to minimize the discrepancies due to test errors. The mean values of the stiffness and moment restraint coefficients are found to be 1.18 and 1.22, respectively, and the corresponding standard deviation is 0.14 and 0.095. The level of scatter in the experimental results is deemed acceptable. For the sake of simplicity and conservative consideration, finally the stiffness restraint coefficient (ξ_s) and moment restraint coefficient (ξ_m) are determined as 1.1 and 1.15, respectively.

6 Check of boundary members

6.1 Check of blind bolted end plate joint

The moment resistance of the blind bolted end plate joints to CFST columns should be checked with [54, 55]:

$$\max\left\{M_{ju}, M_{bi,l}, M_{bi,r}\right\} \le M_{bu} \tag{18}$$

$$M_{bu} = \gamma_b W_{nx} f_{y,b} \tag{19}$$

where M_{bu} is the moment capacity of the steel beam; γ_b is the plasticity development factor and equals 1.05 for H-shaped steel beam in accordance with GB50017 [55]; W_{nx} and $f_{y,b}$ are the net section modulus and the yield strength of the steel beam; M_{ju} is the moment resistance of the blind bolted end plate joints given in Table 5.

In Table 5, the tensile capacity of the bolt component, $F_{t,j}$, is controlled by the failure of the steel tubular wall, the end plate or the bolt (Fig. 15). The bolt component would reach its tensile capacity

when any of the three failure modes occurs. Thus, it can be calculated as follows [26, 34, 52, 56, 57]:

$$F_{t,j}=\min\begin{cases}\dfrac{2f_{y,c}t_c^2}{1-\beta}\left[(\eta-\gamma)+2\sqrt{(1-\gamma)(1-\beta)}\right]\\ f_{y,c}t_c^2\left[\pi(1-\dfrac{\gamma}{2(1-\beta)})+2\dfrac{\beta+\eta-\gamma}{1-\beta}\right]\\ (5.5-0.021m_{ep}+0.017e_{ep})t_{ep}^2 f_{y,ep}\\ (2A_{bo}f_{y,bo}+60f_{bd}A_s)/\gamma_{bo}\end{cases} \tag{20}$$

where $\beta=X_B/(h_c-t_c)$; $\eta=Y_B/(h_c-t_c)$; $\gamma=d_0/(h_c-t_c)$; Y_B is the vertical spacing between bolts; $f_{y,c}$, $f_{y,ep}$ and $f_{y,bo}$ are respectively the yield strength of steel tubular column, end plate and bolt; e_{ep} is the distance between the centre of bolt hole and the edge of end plate; f_{bd} is the design ultimate bond strength and can be determined according to the Section 6.1.3 in fib Model Code [57]; A_s is the area of the anchor reinforcement; γ_{bo} is the reduction factor for considering bolt prying force and equals 1.33.

The compressive bearing capacity of the joints, $F_{c,j}$, is controlled by the steel tubular column wall and steel beam (Fig. 15). When one of these reaches yielding or buckling, the joint is considered to have reached the yield state. So the compressive bearing capacity of the joints can be obtained as [26, 34, 52]:

$$F_{c,j}=\min\begin{cases}8.5A_{eff}f_{y,c} & \\ t_{bf}b_{bf}f_{y,bf} & b_{bf}/t_{bf}<22\sqrt{235/f_{y,bf}}\\ 22t_{bf}^2 f_{y,bf}\sqrt{235/f_{y,bf}} & b_{bf}/t_{bf}\geq 22\sqrt{235/f_{y,bf}}\end{cases} \tag{21}$$

where A_{eff} is the effective zone of the bolt pressure in column wall and can be taken as the bolt hole circumference area within 0.5 times diameter of the bolt; t_{bf} and b_{bf} are respectively the thickness and width of the steel beam flange; $f_{y,bf}$ is the yield strength of the steel beam flange.

6.2 Check of steel beam

The distribution of internal force along the length of the steel beam should be determined to

check the beam strength. For the blind bolted end plate CFST frames infilled with beam-connected SPSWs, the moment varied at different locations within the span of a beam, as shown in Fig. 13. The moment distribution in the beam can be divided into three zones and the moment in each zone can be expressed as follows based on mechanical equilibrium:

$$M_{bi}(x)=\begin{cases} M_{bi,l}+V_{bi,l}x+0.5q_{y(i+1)}x^2 & 0<x\le L_{bi}-L_i \\ M_{bi,l}+V_{bi,l}x+0.5q_{y(i+1)}x^2-0.5q_{yi}(x+L_i-L_{bi}) & L_{bi}-L_i<x\le L_{i+1} \\ V_{bi,r}(L_{bi}-x)-M_{bi,r}-0.5q_{yi}(L_{bi}-x)^2 & L_{i+1}<x\le L_{bi} \end{cases} \tag{22}$$

The shear force at the beam end ($V_{bi,l}$, $V_{bi,r}$) in Eq (22) is given as

$$\begin{aligned} V_{bi,l}&=\left[-(M_{bi,l}+M_{bi,r})-q_{y(i+1)}L_{i+1}(L_{bi}-0.5L_{i+1})+0.5q_{yi}L_i^2\right]/L_{bi} \\ V_{bi,r}&=\left[(M_{bi,l}+M_{bi,r})+q_{yi}L_i(L_{bi}-0.5L_i)-0.5q_{y(i+1)}L_{i+1}^2\right]/L_{bi} \end{aligned} \tag{23}$$

Moreover, the axial fore in the beam is obtained as

$$N_{bi}(x)=\begin{cases} -0.5(q_{xi}L_i-q_{x(i+1)}L_{i+1})-q_{x(i+1)}x & 0<x\le L_{bi}-L_i \\ 0.5(q_{xi}L_i+q_{x(i+1)}L_{i+1})-q_{xi}L_{bi}+(q_{xi}-q_{x(i+1)})x & L_{bi}-L_i<x\le L_{i+1} \\ 0.5(q_{xi}L_i-q_{x(i+1)}L_{i+1})-q_{xi}L_{bi}+q_{xi}x & L_{i+1}<x\le L_{bi} \end{cases} \tag{24}$$

Note that herein the moment in the beam is defined as positive if it is "sagging", i.e. when the lower part of the beam is in tension; the shear force is defined as positive if it has the tendency to shear clock-wise, and tensile axial force is positive. The parameters L_i and L_{i+1} in Eqs. (22) – (24) can be obtained using Eq. (9).

The section strength of the steel beam can be checked by [55]:

$$\frac{N_{bi}}{N_{bu}}+\frac{M_{bi}}{M_{bu}}\le 1 \tag{25}$$

where $N_{bu}=f_{y,b}A_b$; A_b is the cross-sectional area of steel beam; M_{bi} and N_{bi} are respectively the maximum moment in the *i*-th story beam and the corresponding axial force at the same position.

6.3 Check of CFST column

The linear interaction formula has been applied for the capacity checking of CFST columns against failure in terms of section yielding and in-plane instability in accordance with GB50396

[58].

The check of strength capacity of CFST column can be made with

$$\frac{N_{ci}}{N_{cu}}+\frac{M_{ci}}{M_{cu}}\le 1 \tag{26}$$

$$N_{cu}=f_{sc}A_{sc} \tag{27}$$

$$M_{cu}=\gamma_c f_{sc}W_{sc} \tag{28}$$

where $A_{sc}=A_s+A_c$; $f_{sc}=(1.212+B\chi+C\chi^2)f_c$; $\chi=(A_s f_{y,c})/(A_c f_c)$; $W_{sc}=\pi r_0^3/4$; A_{sc}, A_s, and A_c are respectively the cross-sectional area of the CFST column, steel tube and inner concrete; f_{sc}, and f_c are respectively the strength of the CFST column and inner concrete; the cross-sectional shape factor (B and C) and plasticity development factor (γ_c) of the CFST column are listed in Table 6; χ is the confinement factor of the CFST column; W_{sc} is the section modulus of the CFST column; r_0 is the equivalent circular radius and it can be obtained based on the principle of equal area for non-circular cross-sections.

The check of in-plane instability of CFST column is calculated as

$$\frac{N_{ci}}{N_{cu}}+\frac{\beta_m M_{bi}}{1.5M_{cu}(1-0.4N_{ci}/N'_E)}\le 1 \tag{29}$$

where β_m is the equivalent moment factor in accordance with GB50017 [55]; $N'_E=\pi^2 E_{sc}A_{sc}/(1.1\lambda_c^2)$; $E_{sc}=(E_s A_s+E_c A_c)/A_{sc}$; λ_c is the slenderness ratio of the CFST column and equals the calculated length of the member divided by the radius of gyration.

6.4 Experimental validation

In order to verify the feasibility of the above mentioned practical design method for the blind bolted assembly CFST frames with beam-connected SPSWs, representative strain responses at some critical points of the steel beams, steel tubular columns, end plates and SPSWs for specimen CFW1 are presented in Fig. 16.

The strain responses of the intermediate and top steel beam flanges adjacent to the joint regions, shown in Fig 16 (a), were within the yield strain of 1897 με. The strain responses at the base and the first story of steel tubular columns, shown in Fig. 16 (b), all exceeded the yield strain of 1717 με. The extended and flush end plates, shown in Fig. 16 (c), also yielded, and this could be understood also by the marked bending deformation in the extended end plates.

The strains of the SPSWs, shown in Fig. 16 (d), illustrated that the first-story SPSWs remained in an elastic state, owing to the bolt slip that occurred between the SPSWs and the boundary beams. This indicated that a small bolt clearance and a sufficient bolt pretension force should be ensured in the bolted connections in order that the SPSWs fully develop into yielding phase in engineering practice. In addition, Fig. 16 (d) showed that the measured strain value of first story SPSWs was 780 με and the second story SPSWs exceeded yield strain. Therefore, in order to accurately predict the structural responses of the specimen CFW1 and SFW1 using the above mentioned design method, the stress of 140.8 N/mm^2 and yield stress of 281.5 N/mm^2 were respectively used to the diagonal tension field action for the first and second story SPSWs when calculated the distributed horizontal and vertical loads applied along the intermediate and top beams.

Fig. 17 shows a free-body diagram of the two-story, single-bay blind bolted assembly CFST frame with beam-connected SPSWs. In order to assess whether the boundary members of the test specimens satisfied the requirements, the first step is to calculate the initial stiffness (S_{ki}) and moment capacity (M_{ju}) of the blind bolted end plate joints for specimen CFW1 and SFW1 using the test material properties, and the results are shown in Table 7 and 8, respectively. The initial stiffness of the blind bolted joints (S_{ki}) can be determined through Eqs. (12) - (17) and corresponding moment capacity of the joints (M_{ju}) can be obtained according to Eqs. (20), (21) and Table 5. After that, the beam end moments ($M_{bi,l}$, $M_{bi,r}$), shear ($V_{bi,l}$, $V_{bi,r}$) and axial forces ($N_{bi,l}$, $N_{bi,r}$) of the intermediate and top steel beams under partial uniformed distributed load with blind bolted end

plate joints are obtained and are presented in Table 9. Before obtaining those parameters, there is a need to calculate the uniformed distributed loads (q_i and q_{i+1}) acting on the beams from SPSWs using Eqs. (8) – (11). Then, the beam end moments ($M_{bi,l}$, $M_{bi,r}$) can be got following Eqs. (5) – (7); the shear ($V_{bi,l}$, $V_{bi,r}$) and axial forces ($N_{bi,l}$, $N_{bi,r}$) can be determined through Eqs. (23) and (24), respectively. Finally, the maximum moments (M_{bi} (x)) in the intermediate and top beams and the corresponding axial forces (N_{bi} (x)) at the same position can be easily calculated following Eqs. (22) and (24). It can be seen that the maximum moments in the intermediate and top beams are respectively located 588 mm and 1004 mm from the left end of the beams according to Eq. (22).

On the basis of the principle of mechanical balance, the maximum moments and axial forces at the base of CFST columns can also be calculated, and the results of beam and column checks are shown in Table 10 and 11. These results indicate that the moment resistance of the blind bolted end plate joints and the cross-sectional strength of the intermediate steel beams satisfy the requirements according to Eqs. (18) and (25), while the cross-sectional strength ratio of the top steel beams at the maximum moment location, and the ratio of the CFST columns at the base position, are all larger than 1.0 and therefore do not satisfy the requirements according to Eqs. (25) and (26).

The computed results suggest that the plastic deformation may develop at the end plates, the top beams and the bases of CFST columns. From the test observation, the end plates deformed shown in Fig. 6 (c) and Fig. 7 (c); bending deformation appeared at the top steel beams whereas no visible deformation on intermediate beams, as depicted in Fig. 6 (a, b) and Fig. 7 (a, b); welding seam fracture occurred at the CFST column base illustrated in Fig. 6 (d) and Fig. 7 (d). The above results confirm that the design procedures are effective for the blind bolted end plate CFST frames with infill SPSWs connected to beam only.

7 Conclusions

A systematic study of the blind bolted assembly CFST frames with beam-connected SPSWs has been carried out, using both experimental and analytical approaches. The main results and conclusions are summarised as follows:

(1) The main failure modes of the blind bolted assembly CFST frames with beam-connected SPSWs can be summarized as including: a) buckling deformation of SPSWs; b) deformation of end plates and fish plates; c) local buckling at beam bottom flanges; and d) fracture at the CFST column base. The experimental observation on the delayed engagement of SPSWs in the test frames suggests that the bolt clearance should be kept small, while a sufficient bolt pretension force should be applied in bolted connections between the beams and SPSWs to enable full mobilization of the SPSWs into yielding in engineering practice.

(2) Experimental results of two blind bolted assembly CFST frames with infill SPSWs connected to beam only, in comparison with their bare counterparts reported in a previous paper, demonstrated superior performances of the SPSW-infilled frames. The stiffness, strength and energy dissipation capacity of the SPSW-infilled frames improved significantly as compared to the bare blind bolted CFST frames. The results showed that the presence of SPSWs can compensate effectively the relatively small lateral stiffness of the bare blind bolted CFST frames. It has also been found that the column section type had little influence on the seismic performance of the SPSW infilled frame system in terms of the stiffness, strength, ductility and energy dissipation.

(3) Considering semi-rigid characteristics of the joints, the moments at the beam ends in a blind bolted end plate CFST frames with beam-connected SPSWs have been derived, with the effects from the SPSWs being represented by two partial vertical loads on the beam. The stiffness and moment restraint coefficient of the blind bolted end plate joints for curved end plates have also been determined based on previous experimental results.

(4) A practical design method for the blind bolted end plate CFST frames with beam-connected

SPSWs has been summarized for checking the strength of the blind bolted end plate joints, steel beams and CFST columns. The method has been verified by the experimental results in terms of the deformation of end plates and top beams, the fracture of CFST column base and the measured strain responses at key points.

Acknowledgements

The reported research was funded by the National Natural Science Foundation of China (No. 51478158 and 51178156). This work was also sponsored by the New Century Excellent Talents in Universities of China (No. NCET-12-0838). The authors are grateful for the above financial supports.

References

[1] Sabelli R, Bruneau M. Steel design guide: Steel plate shear walls. American Institute of Steel Construction (AISC); 2012.
[2] Caccese V, Elgaaly M, Chen R. Experimental study of thin steel-plate shear walls under cyclic load. J Struct Eng 1993; 119(2): 573-587.
[3] Qu B, Bruneau M. Capacity design of intermediate horizontal boundary elements of steel plate shear walls. J Struct Eng 2010;136:665-75.
[4] Li CH, Tsai KC, Lin CH, Chen PC. Cyclic tests of four two-story narrow steel plate shear walls. Part 2: Experimental results and design implications. Earthq Eng Struct Dyn 2010; 39: 801-826.
[5] Driver RG, Kulak GL, Kennedy DL, Elwi AE, Cyclic test of four-story steel plate shear wall. J Struct Eng 1998; 124 (2): 112-120.
[6] Berman JW, Bruneau M. Experimental investigation of light-gauge steel plate shear walls. J Struct Eng 2005; 131(2): 259-267.
[7] Qu B, Bruneau M, Lin CH, Tsai KC. Testing of full-scale two-story steel plate shear wall with reduced beam section connections and composite floors. J Struct Eng 2008; 134(3): 364-373.
[8] Li CH, Tsai KC, Chang JT, Lin CH, Chen JC, Lin TH, Chen PC. Cyclic test of a coupled steel plate shear wall substructure. Earthq Eng Struct Dyn 2012; 41: 1277-1299.
[9] Zirakian T, Zhang J. Structural performance of unstiffened low yield point steel plate shear walls. J Constr Steel Res 2015; 112: 40-53.
[10] Purba R, Bruneau M. Experimental investigation of steel plate shear walls with in-span plastification along horizontal boundary elements. Eng Struct 2015; 97(22): 68-79.
[11] Gorji MS, Cheng JJR. Plastic analysis and performance-based design of coupled steel plate shear walls. Eng Struct 2018; 166: 472-484.
[12] Wang M, Borello DJ, Fahnestock LA. Boundary frame contribution in coupled and uncoupled steel plate shear walls. Earthq Eng Struct Dyn 2017; 46: 2355-2380.

[13] Wang M, Yang W. Equivalent constitutive model of steel plate shear wall structures. Thin Wall Struct 2018; 124: 415-429.
[14] Xue M, Lu LW. Interaction of infilled steel shear wall panels with surrounding frame members. Proceeding of Structural Stability Research Council Annual Technical Session. Bethlehem, PA 1994: 339-354.
[15] Xue M, Lu LW. Monotonic and cyclic behavior of infilled steel shear panels. Proceedings of 17th Czech and Slovak International Conference on Steel Structures and Bridges. Bratislava, Slovakia 1994:152-160.
[16] Choi IR, Park HG. Steel plate shear walls with various infill plate designs. J Struct Eng 2009; 135(7): 785-796.
[17] Vatansever C, Yardimci N. Experimental investigation of thin steel plate shear walls with different infill-to-boundary frame connections. Steel Compos Struct 2011; 11(3): 251-271.
[18] Guo LH, Rong Q, Ma XB, Zhang SM. Behavior of steel plate shear wall connected with frame beams only. Int J Steel Struct 2011;11:467-79.
[19] Guo LH, Rong Q, Qu B, Liu JP. Testing of steel plate shear walls with composite columns and infill plates connected to beams only. Eng Struct 2017; 136: 165-179.
[20] Clayton PM, Berman JW, Lowes LN. Subassembly testing and modeling of self-centering steel plate shear walls. Eng Struct 2013; 56(6): 1848-1857.
[21] Clayton PM, Berman JW, Lowes LN. Seismic performance of self-centering steel plate shear walls with beam-connected web plates. J Constr Steel Res 2015; 106: 198-208.
[22] Ozcelik Y, Clayton PM. Strip model for steel plate shear walls with beam-connected web plates. Eng Struct 2017; 136: 369-379.
[23] Ozcelik Y, Clayton PM. Seismic design and performance of SPSWs with beam-connected web plates. J Constr Steel Res 2018; 142: 55-67.
[24] Shekastehband B, Azaraxsh AA, Showkati H, Pavir A. Behavior of semi-supported steel shear walls: Experimental and numerical simulations. Eng Struct 2017; 135: 161-176.
[25] Shekastehband B, Azaraxsh AA, Showkati H. Experimental seismic study on shear walls with fully-connected and beam-connected web plates. J Constr Steel Res 2018; 141: 204-215.
[26] Wang JF, Wang JX, Wang HT. Seismic behavior of blind bolted CFST frames with semi-rigid connections. Structures 2017; 9: 91-104.
[27] Wang JF, Li BB, Wang DH, Zhao CF. Cyclic testing of steel beam blind bolted to CFST column composite frames with SBTD concrete slabs. Eng Struct 2017; 148: 293-311.
[28] Wang JF, Pan XB, Peng X. Pseudo-dynamic tests of assembly blind bolted composite frames to CFST columns. J Constr Steel Res 2017; 139: 83-100.
[29] Wang JF, Wang HT. Cyclic experimental behavior of CFST column to steel beam frames with blind bolted connections. Int J Steel Struct (Accepted).
[30] Elghazouli A, Málaga-Chuquitaype C, Castro J, Orton A. Experimental monotonic and cyclic behaviour of blind-bolted angle connections. Eng Struct 2009; 31: 2540-53.
[31] Mirza O, Uy B. Behaviour of composite beam-column flush end-plate connections subjected to low-probability, high-consequence loading. Eng Struct 2011; 33: 647-62.
[32] Wang ZY, Wang QY. Yield and ultimate strengths determination of a blind bolted endplate connection to square hollow section column. Eng Struct 2016; 111:345-69.
[33] Wang W, Li MX, Chen YY, Jian XG. Cyclic behavior of endplate connections to tubular columns with novel slip-critical blind bolts. Eng Struct 2017; 148: 949-962.
[34] Wang JF, Han LH, Uy B. Behaviour of flush endplate joints to concrete-filled steel tubular

columns. J Constr Steel Res 2009; 65(4): 925-939.
[35] Wang JF, Han LH, Uy B. Hysteretic behaviour of flush endplate joints to concrete-filled steel tubular columns. J Constr Steel Res 2009; 65(8): 1644-1663.
[36] Wang JF, Chen LP. Experimental investigation of extended endplate joints to concrete-filled steel tubular columns. J Constr Steel Res 2012; 79(12): 56-70.
[37] Wang JF, Zhang L, Spencer BF. Seismic response of extended endplate joints to concrete-filled steel tubular columns. Eng Struct 2013; 49(2): 876-892.
[38] Wang JF, Spencer BF. Experimental and analytical behavior of blind bolted moment connections. J Constr Steel Res 2013; 82(82): 33-47.
[39] Wang JF, Zhang N. Performance of circular CFST column to steel beam joints with blind bolts. J Constr Steel Res 2017; 130: 36-52.
[40] Tao Z, Hassan MK, Song TY, Han LH. Experimental study on blind bolted connections to concrete-filled stainless steel columns. J Constr Steel Res 2017; 128: 825-838.
[41] Thai HT, Uy B, Yamesri, Aslani F. Behaviour of bolted endplate composite joints to square and circular CFST columns. J Constr Steel Res 2017; 131: 68-82.
[42] Wang JF, Lu J, Zhang HJ, Zhao CF. Experimental investigation on seismic performance of endplate composite joints to CFST columns. J Constr Steel Res 2018; 145: 352-367.
[43] Dubina D, Dinu F. Experimental evaluation of dual frame structures with thin-walled steel panels. Thin Wall Struct 2014; 78(4): 57-69.
[44] Guo HC, Hao JP, Liu YH. Behavior of stiffened and unstiffened steel plate shear walls considering joint properties. Thin Wall Struct 2015; 97: 53-62.
[45] Guo HC, Li YL, Liang G, Liu YH. Experimental study of cross stiffened steel plate shear wall with semi-rigid connected frame. J Constr Steel Res 2017; 135: 69-82.
[46] ATC-24 Guidelines for cyclic seismic testing of components of steel structures. Redwood City (CA): Applied Technology Council; 1992.
[47] JGJ/T 101-2015. Specification for seismic test of buildings. Beijing: Architecture Industrial Press of China 2015 [in Chinese].
[48] Thorburn LJ, Kulak GL, Montgomery CJ. Analysis of steel plate shear walls Structural Engineering Report No. 107. Edmonton (AB): University of Alberta; 1983.
[49] Xu L, Grierson DE. Computer-automated design of semirigid steel framework. J Struct Eng 1993; 119(6): 1740-1760.
[50] Simões LMC. Optimization of frames with semi-rigid connections. Comput Struct 1996; 60(4): 531-539.
[51] European Committee for Standardisation (CEN). Eurocode 3, Annex J: Design of steel structures joints in building frames. European Committee for Standardization Document CEN/TC250/SC3, Brussels, 1998.
[52] European Committee for Standardisation (CEN). Eurocode 3. Design of steel structures, part 1-8: design of joints (EN 1993-1-8:2005). Brussels; 2005.
[53] Thai HT, Uy B. Rotational stiffness and moment resistance of bolted endplate joints with hollow or CFST columns. J Constr Steel Res 2016; 126:139-152.
[54] Wang JF, Li GQ. A practical design method for semi-rigid composite frames under vertical loads. J Constr Steel Res 2008; 64(2): 176-189.
[55] GB50017-2003 Code for design of steel structures. Beijing: China Planning Press; 2003 [in Chinese].
[56] Ghobarah A, Mourad S, Korol RM. Moment-rotation relationship of blind bolted connections

for HSS columns. J Constr Steel Res 1996; 40(1): 63-91.
[57] CEB. CEB-FIP model code 2010. fib model code concrete structures. 2010, Lausanne, Switzerland; 2013.
[58] GB50936-2014 Technical code for concrete-filled steel tubular structures. Beijing: China Planning Press; 2014 [in Chinese].

Captions for Figures

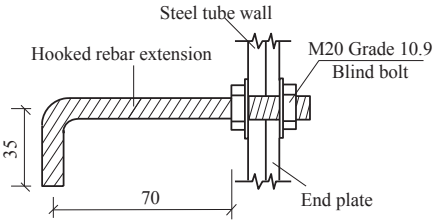

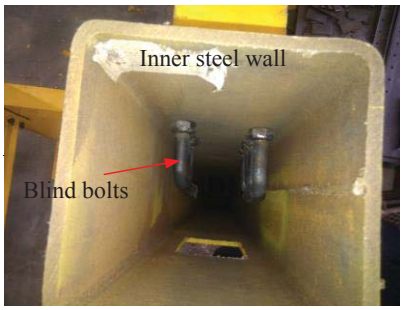

(a) Blind bolt (b) Blind bolt in the tube

Fig. 1 Various configurations of blind bolts with extension

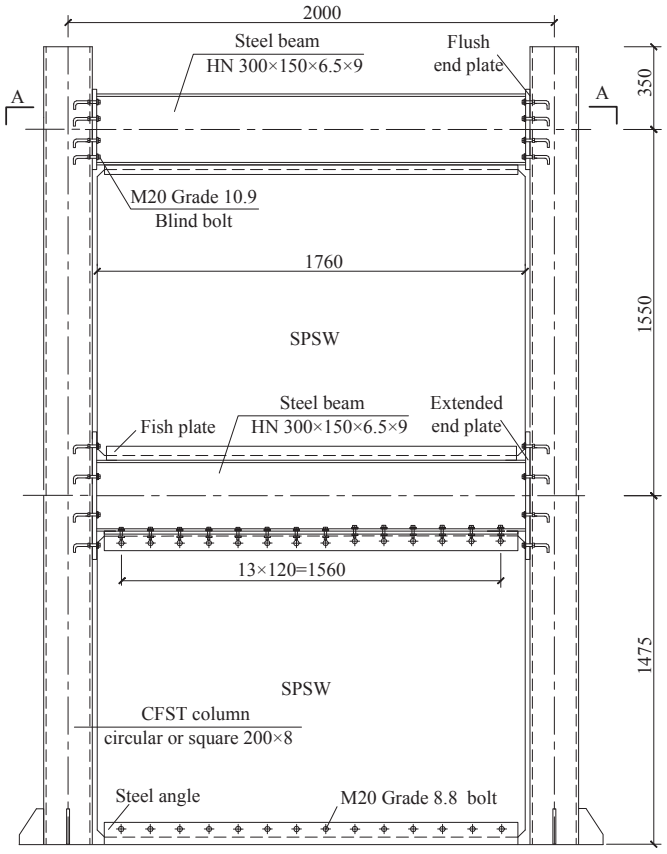

(a) Elevation

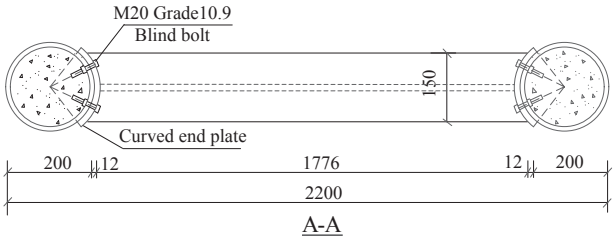

(b) Circular CFST connection

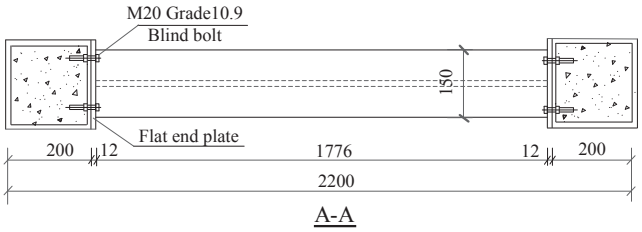

(c) Square CFST connection

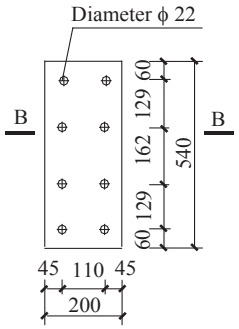

Extended endplate

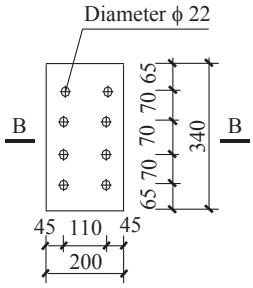

Flush endplate

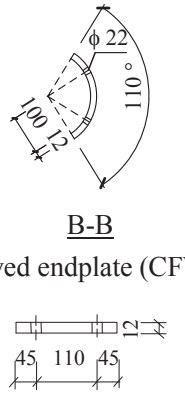

Curved endplate (CFW1)

Flat endplate (SFW1)

(d) Endplate

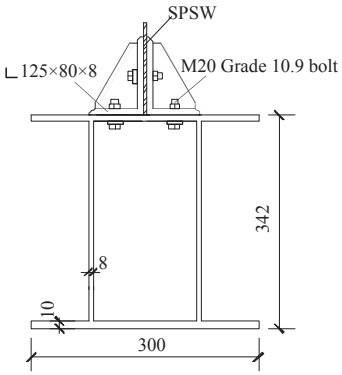

(e) SPSW-base beam connection

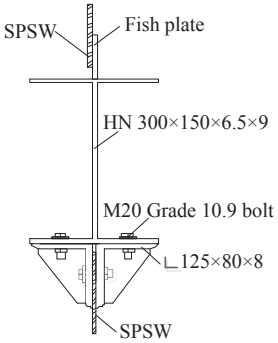

(f) SPSW-intermediate beam connection

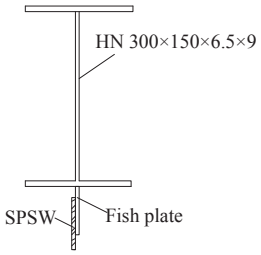

(g) SPSW-top beam connection

Fig. 2 Details of specimens

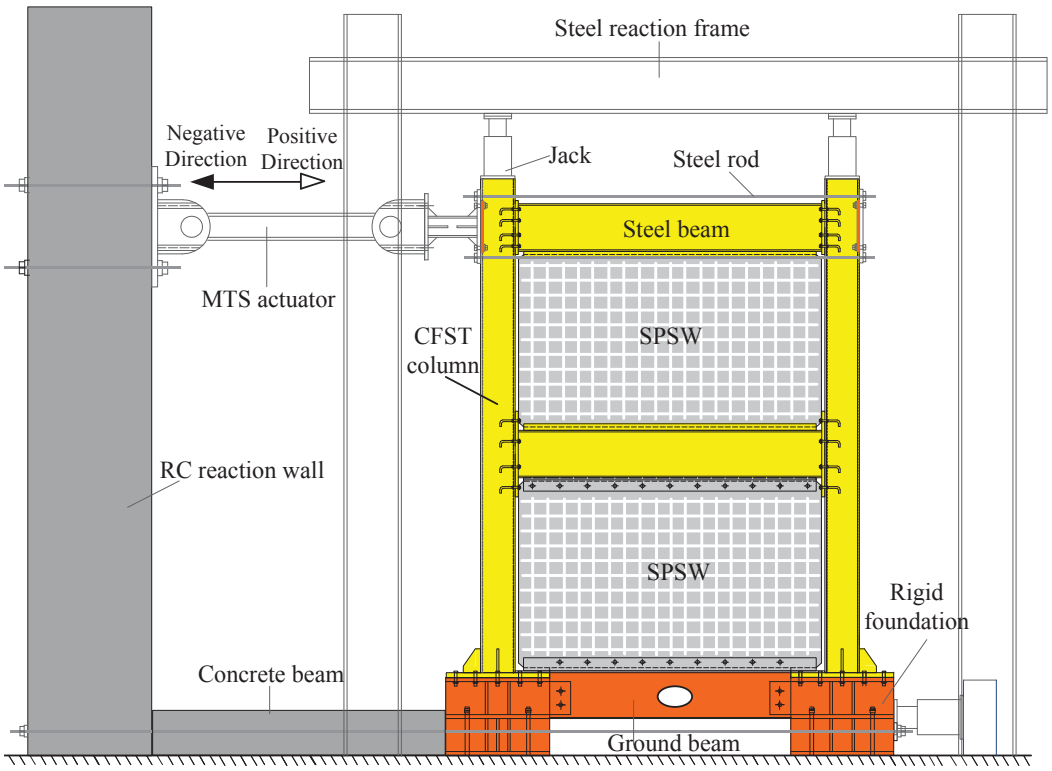

(a) Schematic diagram

(b) On-site photograph

Fig. 3 Test setup

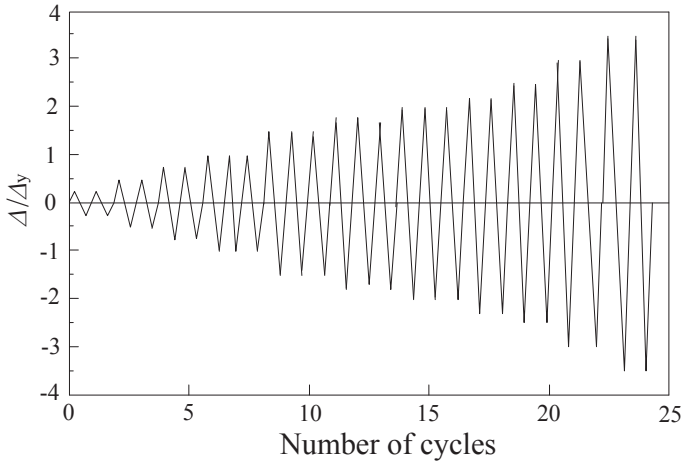

Fig. 4 Loading history for cyclic tests

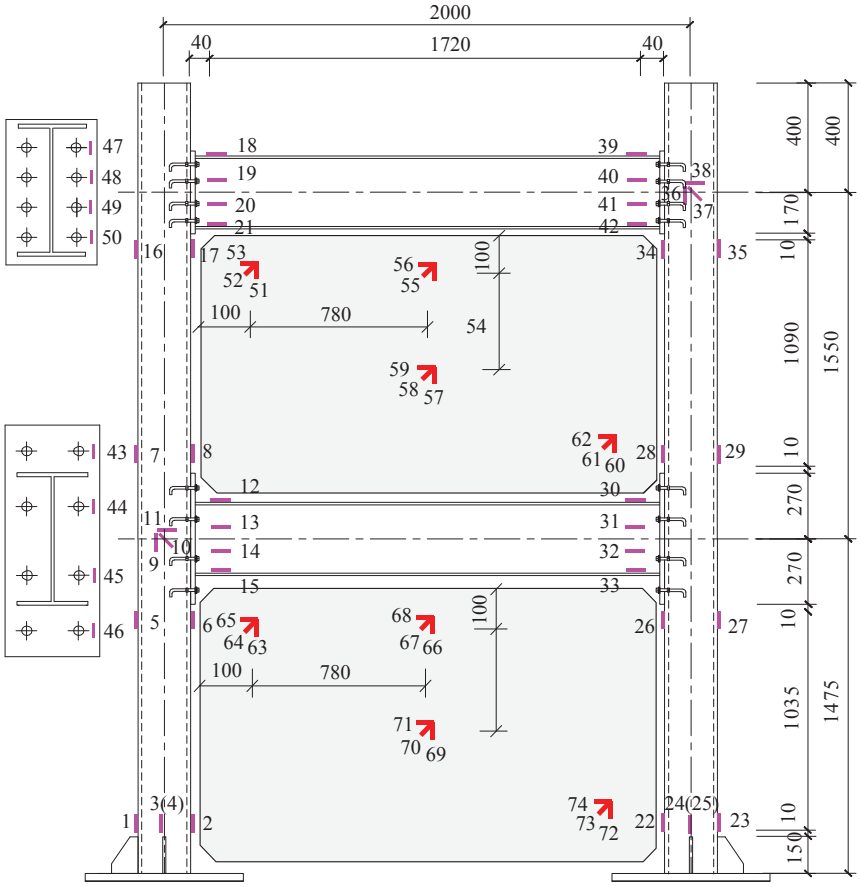

Fig. 5 Layout of strain gauges

(a) Tension strip of SPSW in the first story

(b) Tension strip of SPSW in the second story

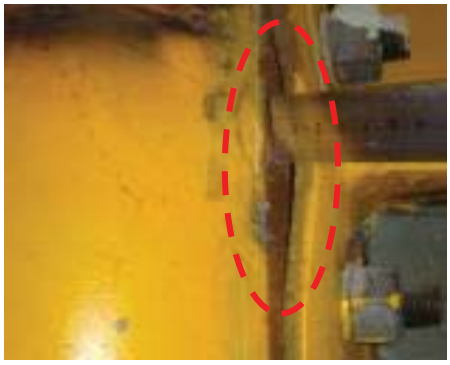

(c) Deformation of extended endplate

(d) Weld fracture at CFST column base

Fig. 6 Failure modes of specimen CFW1

Note: These photos were taken as the specimen reached the drift of 2.32%.

(a) Tension strip of SPSW in the first story

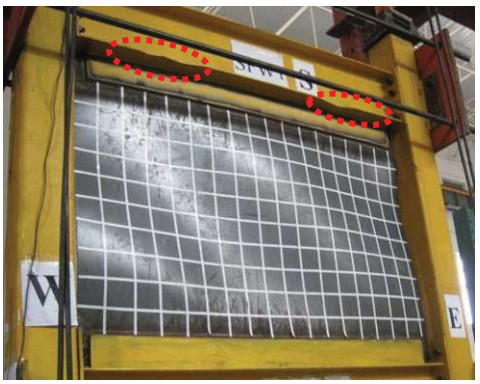

(b) Tension strip of SPSW in the second story

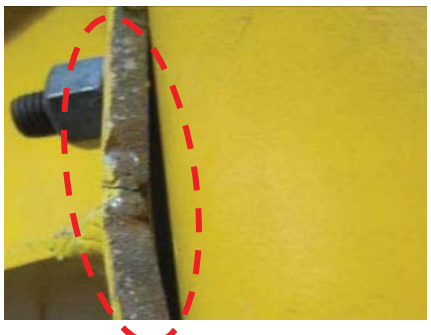

(c) Deformation of extended endplate

(d) Weld fracture at CFST column base

Fig. 7 Failure modes of specimen SFW1

Note: These photos were taken as the specimen reached the drift of 1.98%.

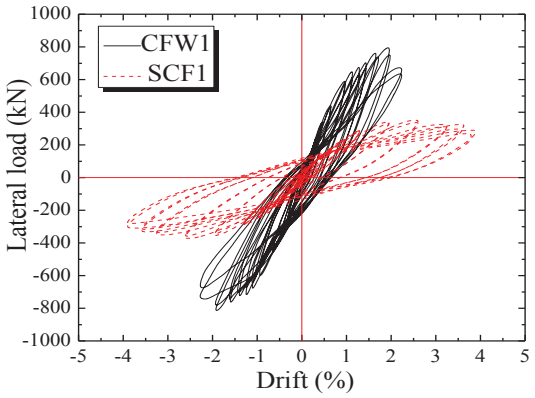

(a) Specimen CFW1and SCF1

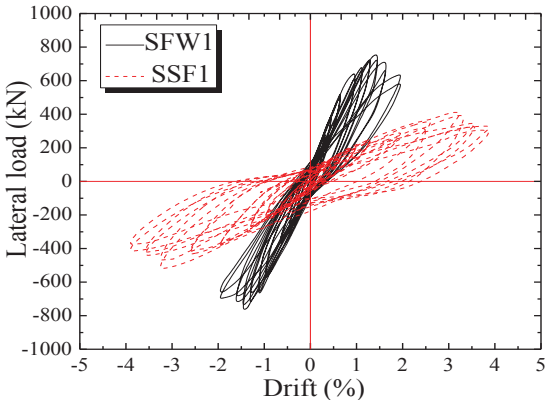

(b) Specimen SFW1and SSF1

Fig. 8 Lateral load - drift hysteretic curves of test specimens

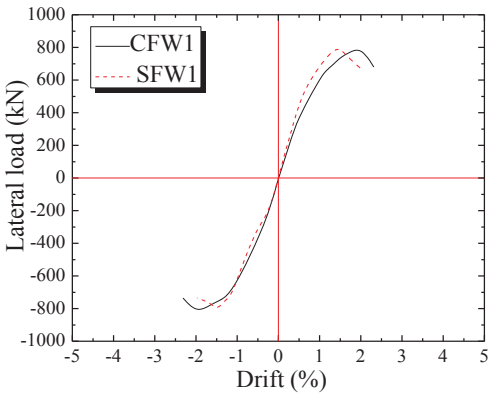

(a) Specimen CFW1and SFW1

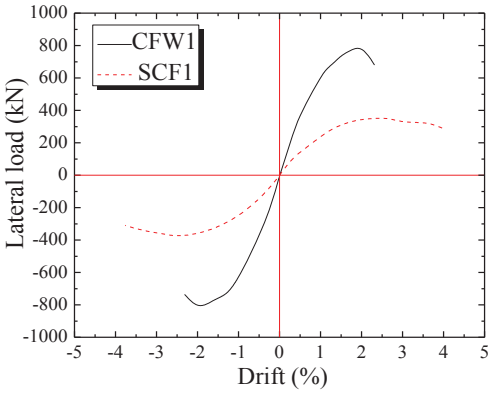

(b) Specimen CFW1and SCF1

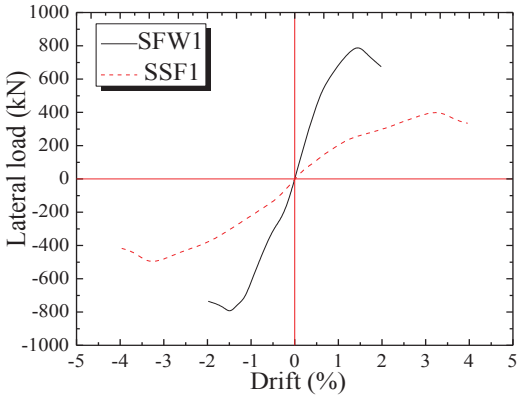

(c) Specimen SFW1and SSF1

Fig. 9 Lateral load - drift skeleton curves of test specimens

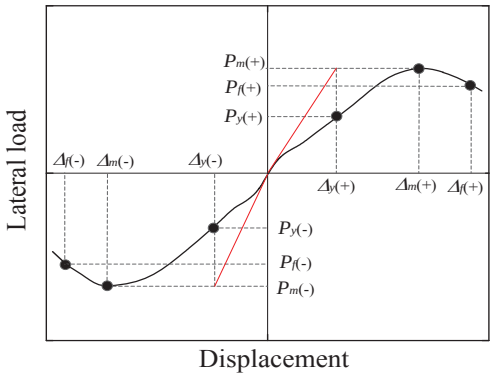

Fig. 10 Feature points of skeleton curves

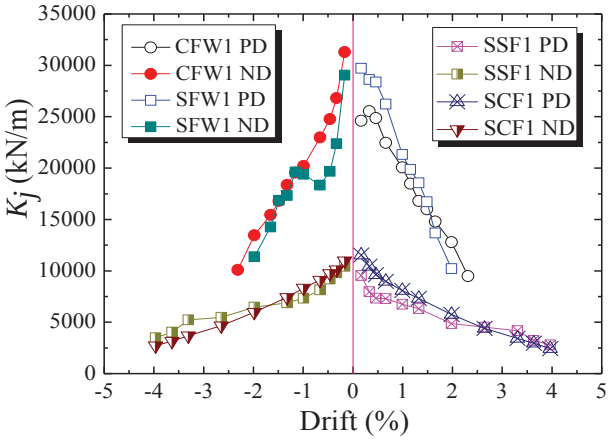

Fig. 11 Stiffness degradation coefficient

Note: 'PD' and 'ND' mean 'Positive Direction' and 'Negative Direction', respectively

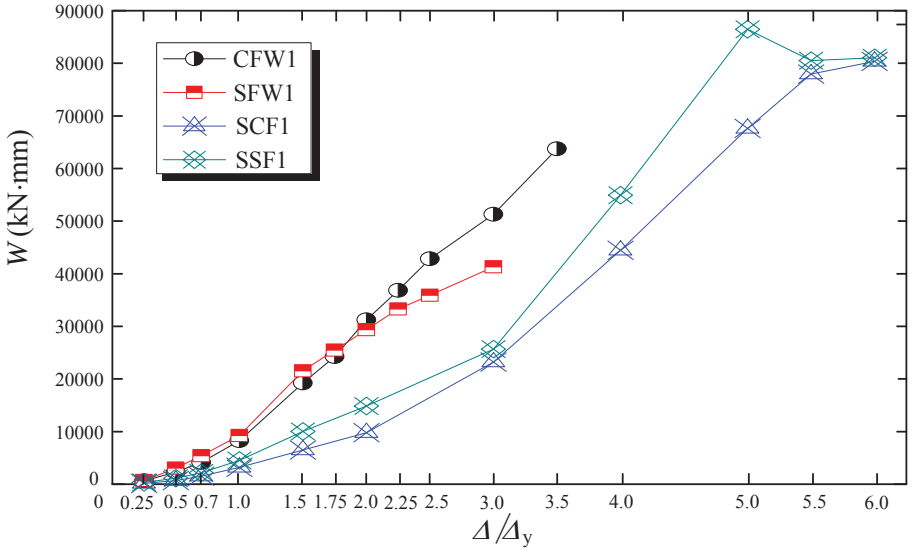

Fig.12 Comparison of the hysteretic energy dissipation capacities

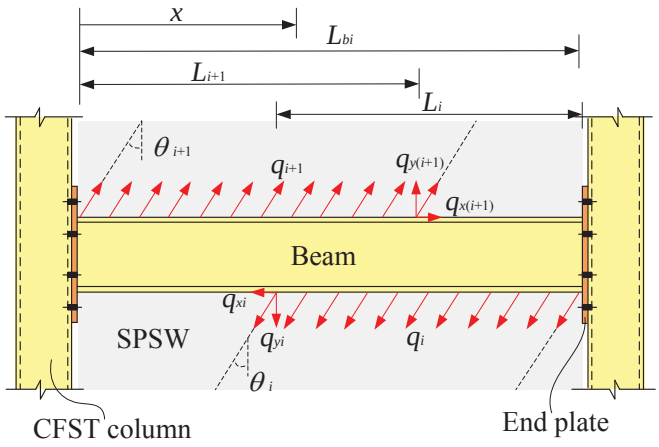

Fig. 13 Mechanical model of partial tension field in beams in a frame with beam-connected SPSWs

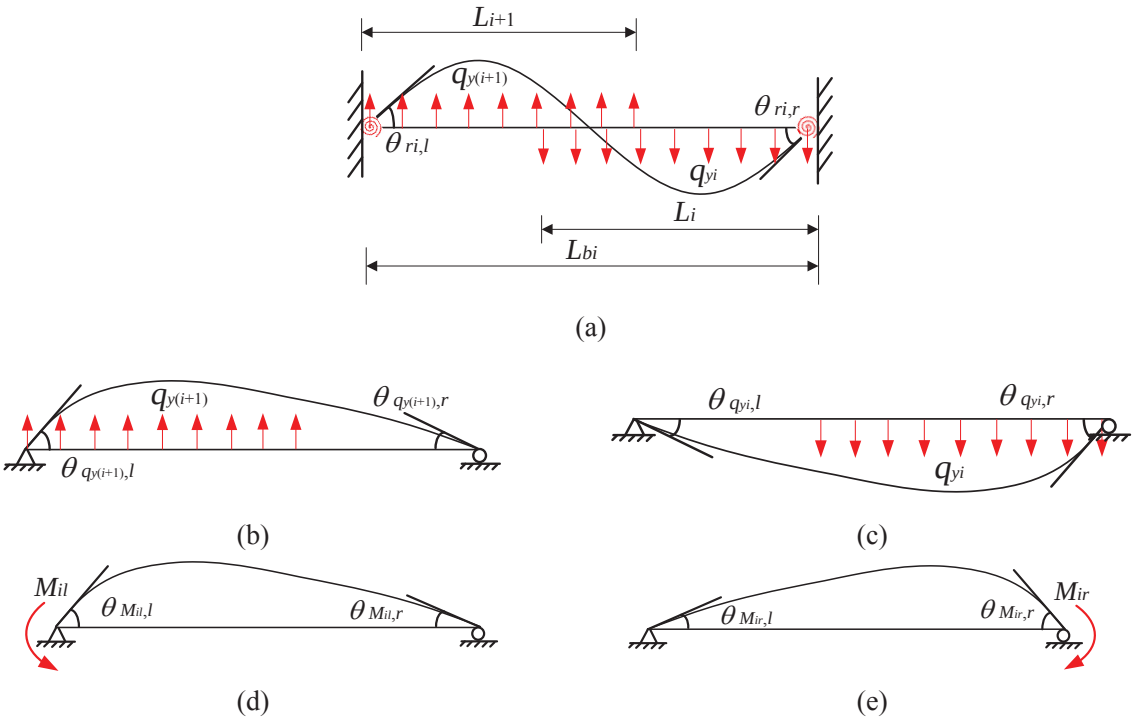

Fig. 14 Illustration of beam end rotation with blind bolted endplate joints

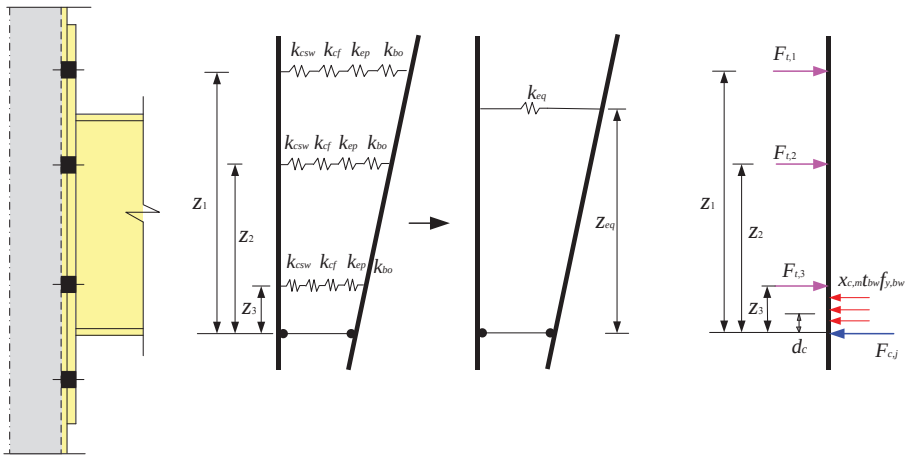

(a) Extended endplate joint

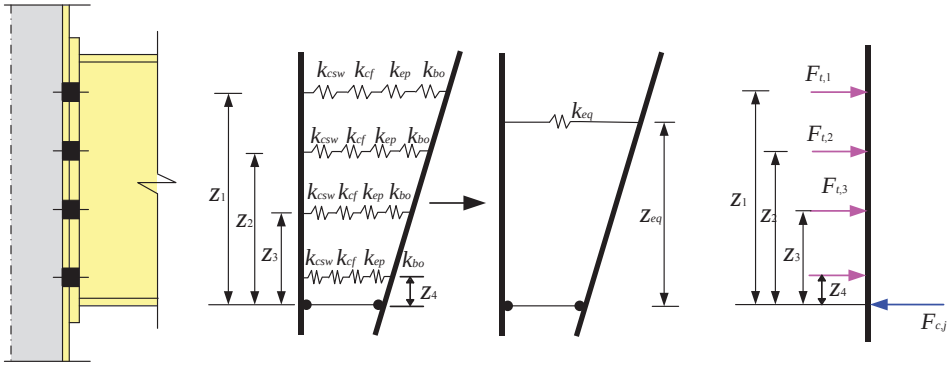

(b) Flush endplate joint

Fig. 15 Analytical model for a blind bolted endplate joint

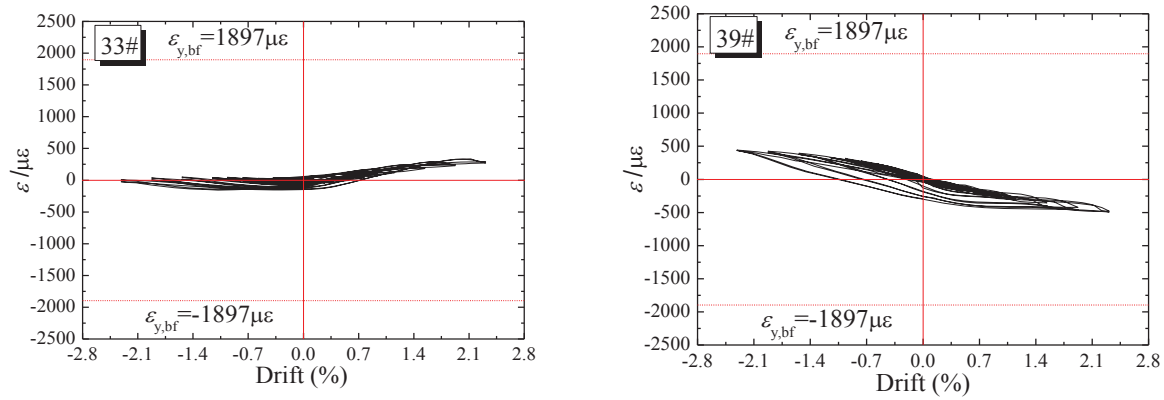

(a) Strain of beam flange

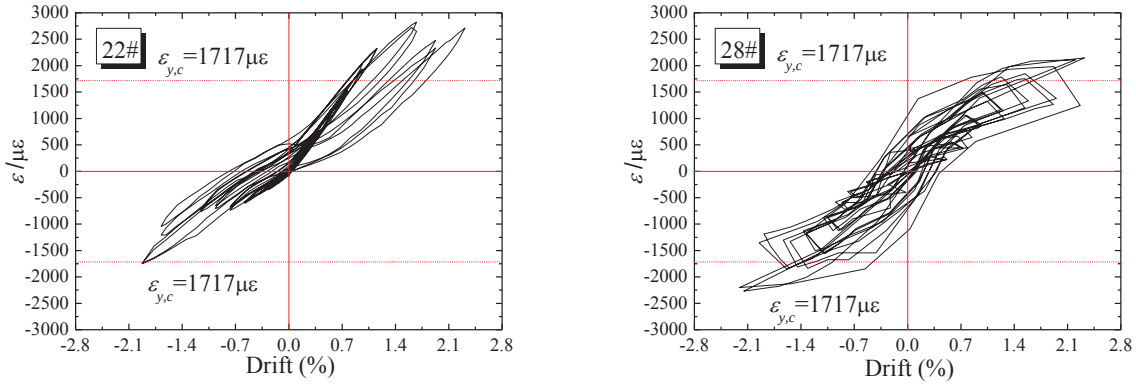

(b) Strain of steel tubular column

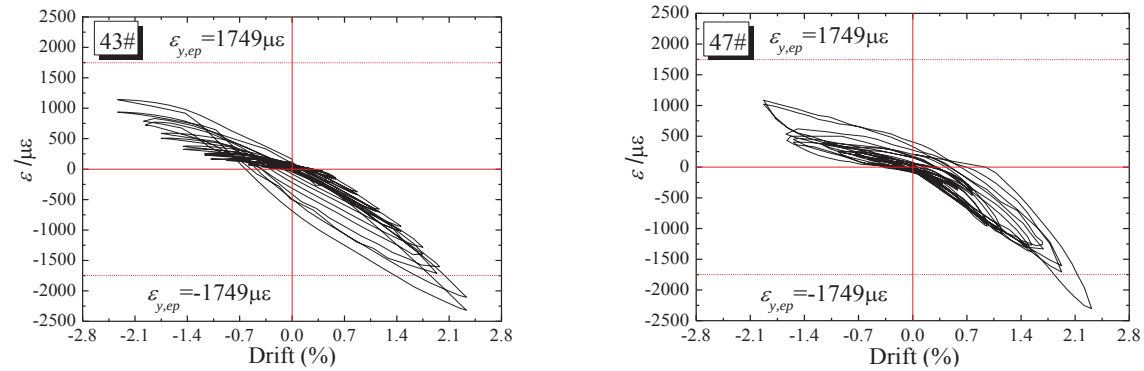

(c) Strain of endplate

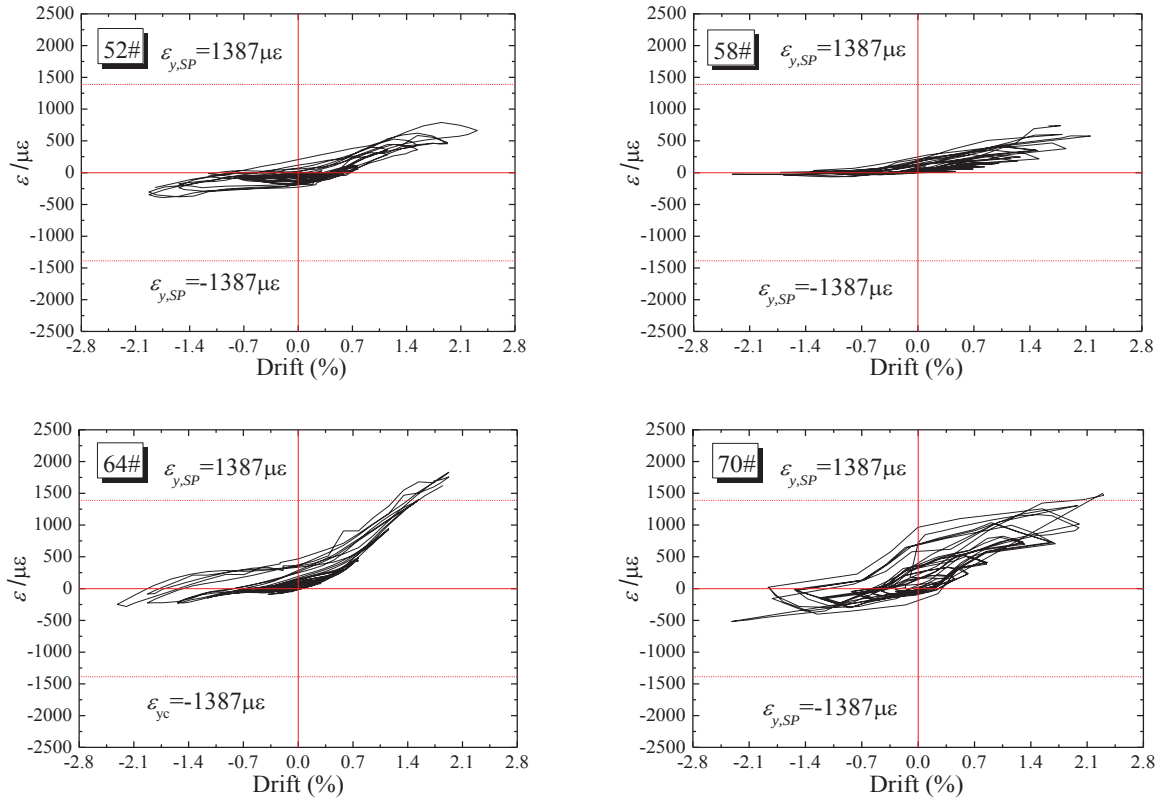

(d) Strain of SPSW

Fig.16 Strain response of main parts in specimen CFW1

Note： $\varepsilon_{y,bf}$, $\varepsilon_{y,c}$, $\varepsilon_{y,ep}$ and $\varepsilon_{y,SP}$ are respectively the yield strain of the steel beam flange, steel tubular column, endplate and SPSW.

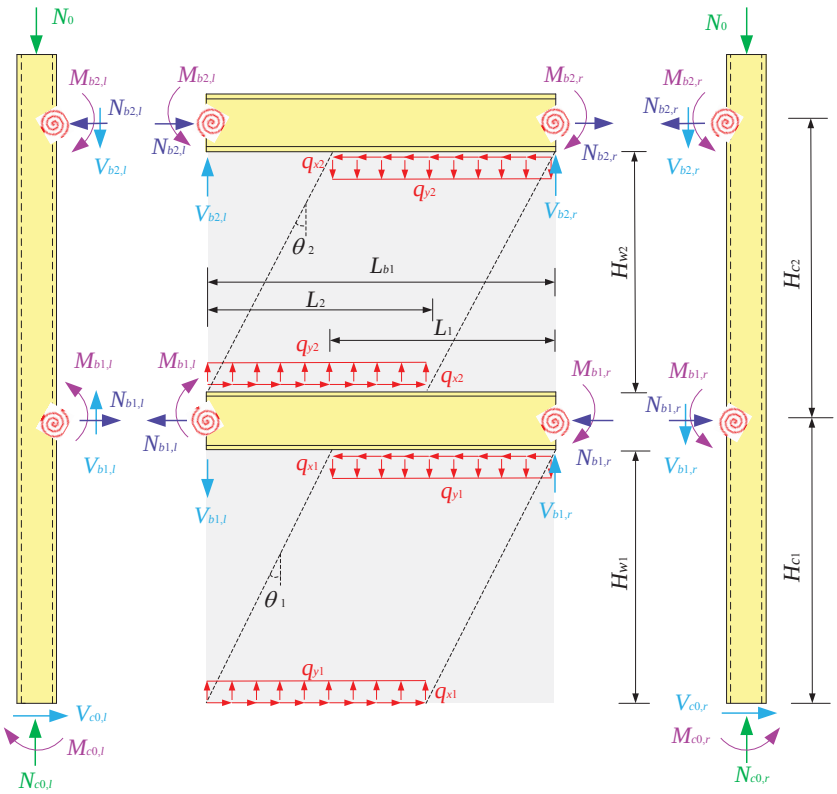

Fig. 17 Free-body diagram of test specimen

Captions for Tables

Table 1. Summary of specimen information

Specimen	Storey	Height (mm)	Column section $h_c \times t_c$ (mm)	Beam section $h_b \times b_{bf} \times t_{bw} \times t_{bf}$ (mm)	Endplate type	SPSW-beam connection	SPSW thickness (mm)
CFW1	1st story	1475	○ 200×8	300×150×6.5×9	Extended endplate	Bolted	5
	2nd story	1550			Flush endplate	Welded	5
SFW1	1st story	1475	□ 200×8	300×150×6.5×9	Extended endplate	Bolted	5
	2nd story	1550			Flush endplate	Welded	5

Table 2. Mechanical properties of steel

Specimen	Thickness (mm)	Yield strength (N/mm^2)	Ultimate strength (N/mm^2)	Young's modulus (N/mm^2)	Elongation at fracture (%)
Steel beam flange	9	381.2	498.5	2.01×10^5	20.3
Steel beam web	6.5	358.1	485.2	2.14×10^5	21.5
Endplate	12	363.8	473.9	2.08×10^5	20.8
Steel tube	8	383.3	485.7	1.97×10^5	20.1
SPSW	5	281.5	475.3	2.03×10^5	21.7

Table 3. Summary of test measurement results

Specimen	Yield point			Maximum point			Failure point			Ductility ratio μ
	P_y (kN)	Δ_y (mm)	Story drift (%)	P_m (kN)	Δ_m (mm)	Story drift (%)	P_f (kN)	Δ_f (mm)	Story drift (%)	
CFW1 (+)	585.1	28.8	0.95	802.8	60.7	2.01	682.4	70.1	2.32	2.43
CFW1 (-)	620.5	29.4	0.97	827.4	59.9	1.98	736.3	70.0	2.31	2.38
SFW1 (+)	602.8	25.3	0.84	798.1	44.9	1.48	678.4	58.5	1.94	2.31
SFW1 (-)	558.0	26.4	0.87	808.5	45.5	1.50	735.7	59.9	1.98	2.27

Note: '(+)' and '(-)' mean 'Positive Direction' and 'Negative Direction', respectively.

Table 4. Restraint coefficient of curved endplates for blind bolted joints

Reference	Connection details		Initial Stiffness		Maximum moment		Notes
			Flush endplate	Extended endplate	Flush endplate	Extended endplate	
Wang et al. [34]	CFST column: □200×8 ○219×8 Steel beam: 300×150×6.5×9		1.398 (t_{ep}=18) 1.302 (t_{ep}=12)	—	1.256 (t_{ep}=18) 1.244 (t_{ep}=12)	—	Monotonic test
Wang et al. [35]	CFST column: □200×8 ○219×8 Steel beam: 300×150×6.5×9		1.429 (t_{ep}=18) 1.299 (t_{ep}=12)	—	1.048 (t_{ep}=18) 1.245 (t_{ep}=12)	—	Cyclic test
Wang et al. [36]	CFST column: □200×10 ○200×10 Steel beam: 300×150×6×10		—	1.052 (t_{ep}=18) 1.304 (t_{ep}=12)	—	1.161 (t_{ep}=18) 1.156 (t_{ep}=12)	Monotonic test
Wang et al. [37]	CFST column: □200×10 ○200×10 Steel beam: 300×150×6×10		—	1.105 (t_{ep}=18) 1.412 (t_{ep}=12)	—	1.070 (t_{ep}=18) 1.592 (t_{ep}=12)	Cyclic test
Wang et al. [38,39]	CFST column: □300×10 ○300×10 Steel beam: 440×290×8×13	t_{ep}=8	1.041	1.508	1.076	1.269	Monotonic analysis of FE
		t_{ep}=20	1.056	1.148	1.206	1.239	
		f_y=235	0.981	1.157	1.142	1.068	
		f_y=345	1.024	1.165	1.193	1.195	
		P_b=0.6	1.084	1.098	1.424	1.461	
		P_b=0.8	1.093	1.102	1.316	1.284	
		d_{bo}=20	1.061	0.978	1.202	1.386	
		d_{bo}=24	1.145	1.029	1.191	1.209	
Tao et al. [40]	CFST column: □360×6 ○360×6 Steel beam:304×165×6.1×10.2		1.384	—	1.160	—	Monotonic test, Composite joints
Thai et al. [41]	CFST column: □250×9 ○273.1×9.3 Steel beam:454×190×12.7×8.5		1.032	1.091	1.073	1.135	Monotonic test, Composite joints
Wang et al. [42]	CFST column: □200×10 ○200×10 Steel beam: 300×150×6×10		1.379	1.513	1.515	1.251	Cyclic test, Composite joints
Mean			1.18	1.18	1.21	1.23	—
Std. Dev			0.14	0.14	0.09	0.10	

Note: t_{ep} is the endplate thickness; f_y is the steel strength of steel tubular column and beam; P_b is the bolt pretension force; d_{bo} is the bolt diameter. The ratio of Ref. [40] was from specimen SB1-1 and CB2-1.

Table 5. Three cases for determining the moment capacity of blind bolted endplate joints

Case	The front bolts of (m-1) row are in full tension and the remaining bolts are in full compression	The front bolts of (m-1) row are in full tension, the m row bolts in partial tension	Only the beam bottom flange is in compression
The depth of compression zone	$x_{c,m}=\min\begin{cases}(\sum_{j=1}^{m}F_{t,j}-F_{c,j})/(t_{bw}f_{y,bw})\\ 38t_{bw}\sqrt{235/f_{y,bw}}\end{cases}$	$x_{c,m}=\min\begin{cases}z_m-t_{bf}/2\\ 38t_{bw}\sqrt{235/f_{y,bw}}\end{cases}$	—
The distances of the bolt row j to the centre of beam's bottom flange	$z_{m+1}<x_{c,m}<z_m$	$x_{c,m\text{-}1}<z_m$ and $x_{c,m}>z_m$	—
The distance between centre of compressive zone and edge of endplate	$d_c=\dfrac{x_c t_{bw}f_{y,bw}(x_{c,m}+t_{bf})}{2(x_{c,m}t_{bw}f_{y,bw}+F_{c,j})}$		—
The moment resistance of the blind bolted endplate joints	$M_{ju}=\xi_m\sum_{j=1}F_{t,j}(z_j-d_c)$	$M_{ju}=\xi_m(\sum_{j=1}^{m\text{-}1}F_{t,j}(z_j-d_c)+F_{t,m}(z_m-d_c))$	$M_{ju}=\xi_m\sum_{j=1}F_{t,j}z_j$
The moment restrained coefficient	$\xi_m=\begin{cases}1.0 & \text{for retangular section column}\\ 1.15 & \text{for circular section column}\end{cases}$		

Note: $F_{t,m}=F_{c,j}+x_{c,m}t_{bw}f_{y,bw}-\sum_{j=1}^{m\text{-}1}F_{t,j}$ for the second case; the moment restrained coefficient, ξ_m, was introduced in Section 2; the meaning of remaining symbols was expressed in Section 3.1.

Table 6. The cross-sectional shape factor and plasticity development factor of CFST columns

	Circle section	Square section
B	$0.176f_{y,c}/213+0.974$	$0.131f_{y,c}/213+0.723$
C	$-0.104f_c/14.4+0.031$	$-0.07f_c/14.4+0.026$
γ_c	1.2	$\gamma_c=-0.483\chi+1.926\sqrt{\chi}$

Table 7. Initial stiffness of blind bolted endplate joints for specimen CFW1 and SFW1

	Flat endplate		Curved endplate	
	Extended	Flush	Extended	Flush
k_{csw} (mm)	7.37	7.37	7.37	7.37
k_{cf} (mm)	0.74	0.74	0.73	0.73
k_{ep} (mm)	2.27	2.27	2.40	2.40
k_{bo} (mm)	9.74	9.74	9.74	9.74
z_{eq} (mm)	281.27	187.60	281.27	187.60
k_{eq} (mm)	1.17	1.58	1.18	1.59
S_{ki} (kN·m/mrad)	19.12	11.48	21.09	12.66

Table 8. Moment capacities of blind bolted endplate joints for specimen CFW1 and SFW1

	Flat endplate		Curved endplate	
	Extended	Flush	Extended	Flush
$F_{t,j}$ (kN)	173.46	142.30	162.61	133.72
$F_{c,j}$ (kN)	514.62	514.62	563.34	563.34
$x_{c,m}$ (mm)	2.47	—	—	—
d_c (mm)	0.10	—	—	—
M_{ju} (kN·m)	112.11	81.93	120.90	89.50

Table 9. Beam end moments, shear and axial forces of specimen CFW1 and SFW1

	1st story		2nd story	
	Left side	Right side	Left side	Right side
M_{bi} (N·mm)	9.61×10^{4}	-1.53×10^{3}	-8.35×10^{4}	1.37×10^{5}
V_{bi} (N)	-6.47×10^{5}	3.87×10^{4}	3.77×10^{5}	8.30×10^{5}
N_{bi} (N)	1.66×10^{5}	-1.66×10^{5}	-3.19×10^{5}	3.19×10^{5}

Table 10. Beam check of specimen CFW1 and SFW1

	CFW1		SFW1	
	1st story beam	2nd story beam	1st story beam	2nd story beam
$M_{bi,max}$ (N·mm)	-1.90×10^{8}	3.14×10^{8}	-1.90×10^{8}	3.14×10^{8}
M_{bu} (N·mm)	1.96×10^{8}	1.96×10^{8}	1.96×10^{8}	1.96×10^{8}
N_{bi} (N)	-1.76×10^{5}	-3.25×10^{5}	-1.76×10^{5}	-3.25×10^{3}
N_{bu} (N)	1.81×10^{6}	1.81×10^{6}	1.81×10^{6}	1.81×10^{6}
Check result	0.10	1.78	0.11	1.78

Table 11. CFST column check of specimen CFW1 and SFW1

	CFW1		SFW1	
	Left side column	Right side column	Left side column	Right side column
M_{c0} (N·mm)	-7.21×10^{8}	7.21×10^{8}	-7.21×10^{8}	7.21×10^{8}
M_{cu} (N·mm)	1.95×10^{8}	1.95×10^{8}	1.16×10^{8}	1.16×10^{8}
N_{c0} (N)	-1.06×10^{6}	-2.20×10^{6}	-8.87×10^{5}	-2.02×10^{6}
N_{cu} (N)	4.42×10^{6}	4.42×10^{6}	3.85×10^{6}	3.85×10^{6}
Result	3.93	4.19	6.47	6.77